Investigation of Different Cardboard Materials Under Impact Loads

Philipp Johst,[a,*] Ulrike Kaeppeler,[b,c] Dimitrij Seibert,[a] Michael Kucher,[a] and Robert Böhm [a]

Packaging materials, such as cardboard, must endure vigorous loads during handling and transport, which could lead to damage to the packaged goods. To ensure that the transported goods reach the consumer safely, a profound knowledge of the behavior of packaging materials under impact loads is required. This study experimentally investigated the behavior of two different cardboard materials under impact loads. Different kinetic energy levels were obtained using a specially developed test rig. First, the resulting damage of the specimens was qualitatively characterized based on digital analysis. Second, the damage was quantitatively analyzed using the imprint diameter after impact as the characteristic parameter. It was found that three different damage phenomena occurred on both investigated materials: imprint, cracking, and breakthrough. Different imprint diameters were detected with increasing kinetic energy of the impactor. The impact load resistance of the material with the higher grammage was higher than that of the material with the lower grammage.

DOI: 10.15376/biores.18.1.1933-1947

Keywords: Cardboard; Impact test rig; Impact load resistance; Kinetic impact energies; Damage phenomena; Imprint diameter

*Contact information: a: Leipzig University of Applied Sciences (HTWK Leipzig), Faculty of Engineering, Karl-Liebknecht-Straße 132, Leipzig 04277 Germany; b: Leipzig University of Applied Sciences (HTWK Leipzig), Faculty of Computer Science and Media, Karl-Liebknecht-Straße 132, Leipzig 04277 Germany; c: iP³ Leipzig – Institute for Printing, Processing and Packaging Leipzig, Karl-Liebknecht-Straße 132, Leipzig 04277 Germany; *Corresponding author: philipp.johst@htwk-leipzig.de*

INTRODUCTION

The requirements of packaging have increased exponentially in the most recent years (Weber *et al.* 2022). Packaging systems are designed to protect products from mechanical, biological, chemical, and climatic hazards during the distribution and transportation process. Thus, the products can be shipped to consumers without damage while maintaining the product quality (Corner and Paine 2002; Luong *et al.* 2021; Garbowski *et al.* 2022). In addition to this basic protection function, packaging must provide the ability to individualize and successfully advertise the product (Singh *et al.* 2017; Weber *et al.* 2022). The objective of the packaging development process is to conceptualize packaging for a particular product and to consider the specific requirements (Pålsson 2018).

There are numerous materials available to manufacture packaging systems, such as wood, paper, cardboard, corrugated cardboard, metal, or even plastics (Baumann 2016; Garbowski *et al*. 2020). Among paper and cardboard materials, corrugated cardboard is the

most commonly produced packaging material in Germany. Besides, cardboard is the second most common produced material in the packaging industry (Statista 2022).

For the most part, cardboard is used as a fundamental supply for folding boxes to ensure a safe transport or the shipping of goods (Baumann 2016; Luong *et al.* 2018). Particularly during transport processes, packaging materials have to endure high loads. Consequently, products may be exposed to various incidents during their handling and transport, such as dropping from a higher level, impact-loads, compressions to the mass of other packages, or vibration during the transportation process (Bivainis and Jankauskas 2015; Luong *et al.* 2021). The transported goods are in a packaging box made from cardboard. In the absence of cushioning and securing, these goods may start to move as a result of the previously mentioned transport processes and collide against the packaging material from the inside. This might cause impact damage to the cardboard material.

Commonly identified deficiencies in packaging materials include inappropriate sizes, exceeded performance limits, or low-quality packaging materials (Herzau *et al.* 2010). Therefore, conducting a series of experimental tests and the execution of additional numerical simulations are necessary to prevent and predict damage in cardboard packaging. Transport safety tests are costly, resource-intensive, and are hardly being used in the industry (Weber *et al.* 2022).

While the in-plane elastic-plastic material behavior of cardboard materials is already well known (Coffin *et al.* 2011), the impact behavior of such materials has rarely been investigated to date. For low strain rates, Garbowski *et al*. (2012) analyzed the orthotropic deformation behavior of paper foils by means of biaxial tests. Furthermore, Kaeppeler *et al.* (2022) measured the compaction of cardboard materials. They used an orthotropic elastic constitutive model and Hill yield criterion for the description of the anisotropic plastic deformations to approximate the inelastic deformation behavior. Similar studies were carried out for corrugated cardboard by Ran and Liu (2019) and Mrówczyński *et al.* (2021). To describe the impact behavior of cardboard materials, the orthotropic deformation behavior of these materials at high strain rate must be considered. Furthermore, it should be noted that in impact processes, the dominant loads are oriented in the thickness direction. Hence, local damage is likely. This damage is largely influenced by the material's behavior. Thus, the main intention of this study was to introduce an experimental approach for the determination of the different damage phenomena of cardboard under impact loads, considering all these governing effects. Further, the investigation aims to understand cardboard's impact loading properties as packaging material (Griffin *et al.* 1985). For that reason, this work investigated the damage behavior of different types of cardboard under impact loading using a Multiple-Impact-Test-Rig. This test-rig aims to reflect the effects of impact caused by an unfixed spherical object of a transported good. Bivainis and Jankauskas (2015) explored the impact behavior of corrugated paperboard using puncture resistance tests. It was shown that the puncture energy has strong linear relationship with grammage of corrugated paperboard. However, the necessary kinetic impact energies that cause varying structural damage to the cardboard material have not yet been investigated.

For the following experiments, various kinetic energies were selected, which resulted in different states of damage. The observed damage formed the basis of the digital analysis. This paper compares the structural damage of two different types of cardboard based on the imprint diameter. An assessment of the material's impact behavior and its resistance to impact was provided.

EXPERIMENTAL

Materials

Two types of cardboard materials with different properties were investigated. These were a conventional industrial fresh fiber cardboard Ensocoat (Stora Enso, Imatra, Finland) and Trayforma (Stora Enso, Imatra, Finland), hereinafter referred to as Material A – 330 Fig. 1a) and Material B - 350 (Fig. 1b), respectively.

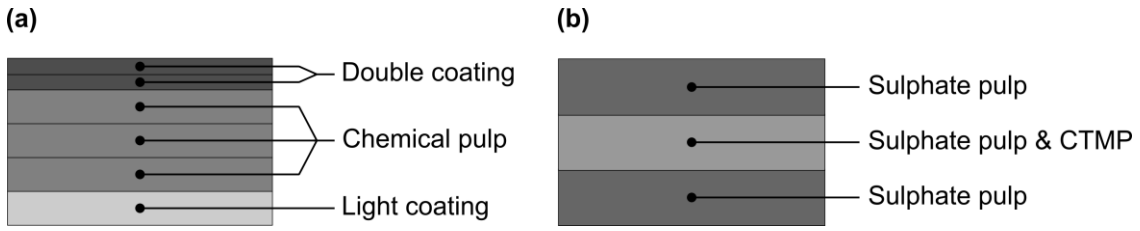

Fig. 1. Structure of: Material A - 330 (a) and Material B - 350 (b)

There is a difference in the fundamental composition of Material A - 330 and Material B - 350. Thus, the layer structure itself and particular structural properties vary. In the production of cardboard, several layers are mechanically pressed together without the use of adhesives. Material A - 330 is considered a solid bleached sulphate (SBS) board with a three-layer-fiber construction of chemical pulp. It is double-coated on the top side with one layer of light coating on the reverse side. The grammage of Material A - 330 is 330 g/m^2 with a thickness of about 401 µm. Conversely, Material B - 350 is designed as a bleached virgin-fiber board with a three-layer fiber structure. The outer layers are made of sulphate pulp and the inner layer made of chemithermomechanical pulp (CTMP). However, only the central layer contains lignin. The grammage of Material B - 350 is 350 g/m^2 with a thickness of about 449 µm. The thickness of both materials were measured following DIN EN ISO 534 (2012) with a thickness tester (Frank Dickenmesser, Frank-PTI GmbH, Birkenau, Germany).

Both materials undergo a similar manufacturing process. Prior to cardboard production, the fibers are an aqueous fiber-water pulp. The pulp is initially fed onto a wire mesh, which is part of the paper machine in the forming section, commonly called the wet end. The wire mesh moves at high speed and thereby is dewatered towards the bottom. This process controls two important characteristics that affect the materials' performance. First, the downward dewatering on the wire mesh results in a top side and a back side (also called wire side) of the material. This becomes important in material testing and therefore it is crucial that the same side of the material is used during experiments as the impacting side. While fines and additives are mostly located at the bottom of the cardboard, long fibers lie on the material's top side. Secondly, the movement of the wire mesh results in an anisotropy of the material properties. This means that the fibers will exhibit a preference for lying along the machine speed direction. Therefore, the mechanical properties of the investigated materials will depend on the direction. The pronounced anisotropy must be taken into account.

Furthermore, it is vital to mention that the fibers differ in their origin, which will also have an impact on the fibers' mechanical properties. For instance, this originates from the various fiber's geometries. The fiber lengths of Material B - 350 have already been investigated in previous studies, such as by Käppeler *et al.* (2020). Fiber lengths of

approximately 20 µm were recorded in the fibers fraction. The fiber lengths and the distribution of the fiber lengths differed only slightly in the outer (a) and inner (b) layers of Material B - 350 (Käppeler *et al.* 2020). The majority of the fiber length was around 1000 µm. The fiber width was considerably smaller. Thus, it is clear that different mechanical properties occur in the material in the three directions when the fibers are aligned in the fiber direction. Similar studies could not be found for Material A - 330. Thus, no direct comparison of the fiber lengths is possible, but the ratios seem to be similar.

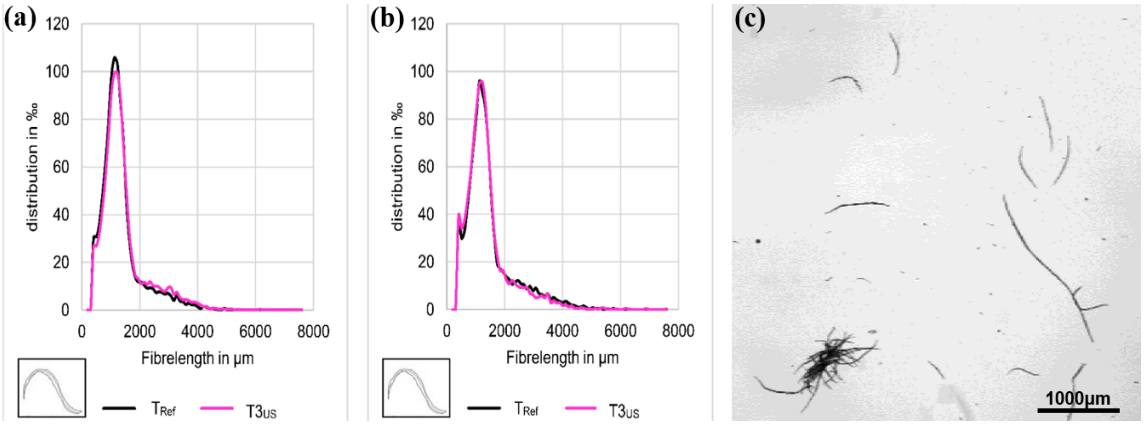

Fig. 2. Fiber length distribution of Material B - 350 (T_{Ref}) in outer layers (a), Fiber length distribution of Material B - 350 (T_{Ref}) in inner layers (b), single fibers in the fiber length measurement process (c). Figure 2 is republished from Käppeler *et al.* (2019) and Käppeler *et al.* (2020) with permission from the authors.

It is well known that the adhesion between the fibers within paperboard is realized *via* hydrogen bonds. These bonds are formed especially at the fibrils of the fibers because the surface area is large. For damage to occur, the hydrogen bonds need to be weakened to an extent that the fiber structure ruptures.

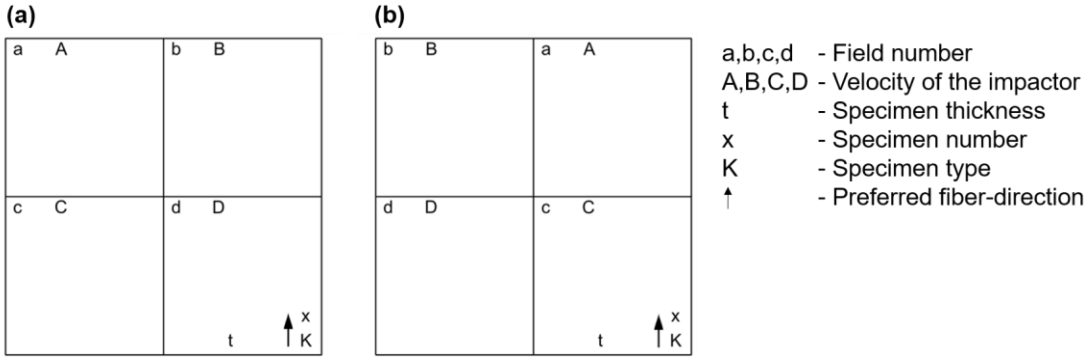

Fig. 3. Top side of the specimen (a); Bottom side of the specimen (b)

Before the experimental testing, the materials were stored for 48 h under standard atmospheric conditions (23 °C ± 1 °C and 50 % ± 2 % humidity) in accordance with ISO 187 (2022). After this conditioning period, the experiments were conducted under the same ambient conditions. Consequently, each specimen of Material A - 330 and Material B - 350 was cut into specimens with a width of 100 mm and a length of 100 mm. Each specimen was later optically divided into four different segments to realize one

impact for each segment (Fig. 3). For these four segments of one specimen, the resulting impact patterns were similar during all measurements.

Multi-Impact-Test-Rig

The effects of dynamic loads on Material A - 330 and Material B - 350 were experimentally simulated with the help of a Multiple-Impact-Test-Rig (Mehrfach-Impact-Prüfstand, Hegewald & Peschke, Nossen, Germany). The experimental setup is shown in Fig. 4.

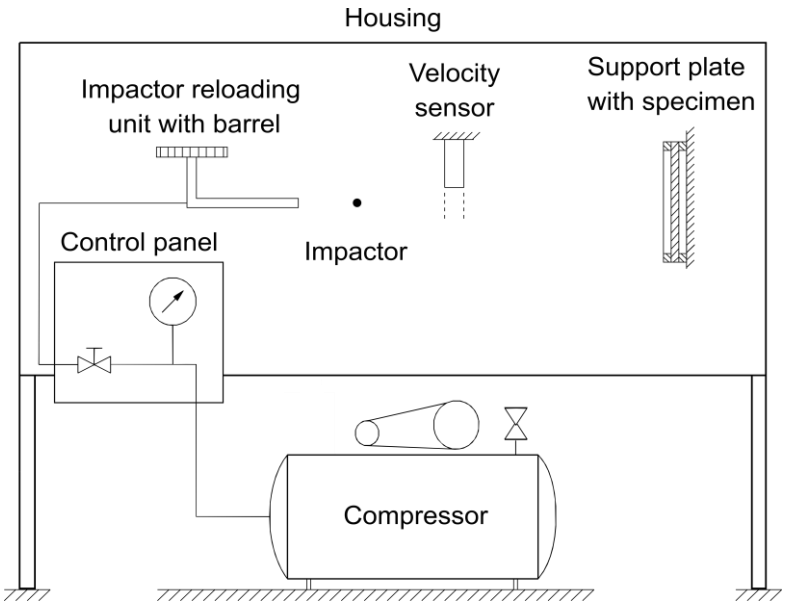

Fig. 4. Experimental setup of the Multiple-Impact-Test-Rig

This test-rig represents an acceleration device using compressed air. It allows the acceleration of three different steel impactors with a mass of 0.26×10^{-3} kg, 0.51×10^{-3} kg, and 0.88×10^{-3} kg to reach velocities in the range of 15 m/s and 50 m/s. The dynamic load of the impactor is adjustable with the help of a control panel. Therefore, the test-rig setup ensures the generation of reproducible deformations on the specimens. For each test, the cardboard specimens were fixed at the same position and aligned in the same preferred fiber direction within a specially developed support plate. The acceleration distance of the impactors is guided in a barrel over a distance of approximately 155 mm. During the experiments, the final velocity of the impactor was measured by a velocity sensor (Ballistischer Chronograph Mod. R2A, TEC-HRO, Brigachtal, Germany). The impactor blocks the light from the velocity sensor. Based on this information, the velocity of the impactor can be determined. After traveling a distance of 150 mm, the impactor hits one selected field of the 100 mm × 100 mm specimen. As mentioned above, the impact load was applied every time on the same surface side of the specimens. While Material A - 330 was impacted on the double coating side, the impactor hit Material B - 350 on the top layer sulphate pulp side (see Fig. 1). To ensure the safety of the experimenter during the tests, the previously mentioned components are placed in a housing.

To determine the damage phenomena of the materials, various velocities leading to different kinetic energies were used. Following first preliminary tests with an equal experimental setup, pressures between 0.05 and 0.30 MPa were applied using the control panel to realize velocities of the impactor between 18 and 44 m/s at the velocity sensor as specific input parameters. No plastic deformation was detected for lower impact velocities than 18 m/s. It is possible that the hydrogen bonds were not weakened in such a way that the fiber structure of the specimens was ruptured. At a higher impact velocity than 44 m/s, no change in the damage behavior of the investigated materials was recordable. For the experiment, the used steel impactor had a diameter of 4 mm and a mass of 0.26×10^{-3} kg. The resulting kinetic energy was determined with Eq. 1,

$$E = 0.5mv^2 \quad (1)$$

where E is kinetic energy (J), m is mass (kg), and υ is the velocity of the impactor (m/s). Table 1 summarizes the performed experimental tests.

Table 1. Experimental Settings of the Parameters Pressure, Number of Impacts, Mean Velocity of the impactor, and the Resulting Mean Kinetic Energy of the Impactor

Settings	**Material A - 330**							
Pressure (MPa)	0.05	0.08	0.09	0.10	0.11	0.12	0.15	0.20
Number of Impacts	20	19	20	18	20	20	18	20
Velocity *u* (m/s)*	18.77	24.59	26.25	27.25	29.28	30.56	33.09	38.24
Kinetic Energy *E* (J)*	0.046	0.079	0.090	0.097	0.112	0.122	0.143	0.191
	Material B - 350							
Pressure (MPa)	0.10	0.13	0.14	0.15	0.16	0.20	0.30	
Number of Impacts	19	17	18	18	16	17	16	
Velocity *u* (m/s)*	27.25	31.55	32.86	33.44	35.33	38.14	44.53	
Kinetic Energy *E* (J)*	0.097	0.130	0.141	0.141	0.163	0.190	0.259	
* These parameters represent the mean values of the performed impacts								

To analyze statistical features, at least 16 specimens with Material A - 330 and Material B - 350 were investigated for each pressure setup. A two-sided t-test ($p = 0.975$) was performed. This allowed the identification of statistical outliers in the kinetic energy of the impactor regarding the pressure setups. These outliers were not considered further in the evaluation, as they can be attributed to the experimental setup.

Digital Analysis

Following the impact test, the specimens' surface was digitally analyzed. The damaged materials were evaluated by taking scans of the damaged areas using a digital 3D-macroscope (Keyence VR3000, Keyence Deutschland GmbH, Neu-Isenburg, Germany). The macroscope enabled structured-light 3D-scans to generate 3D-surface-images. The identified damages on the images were subsequently analyzed with the help of the manufacturer's original software tool Keyence VR-3000 G2 Series Analyzer (Version 2.5.0.332, Keyence Deutschland GmbH, Neu-Isenburg, Germany). The evaluations allowed the comparison of the effects on the damage phenomena, as a result of the different impact loads.

To quantify the remaining deformation of the specimen, the imprint diameter was measured. Thereby, the diameter was determined from the mean value of the vertical (Fig. 5a) and horizontal profile measurement (similar to Fig. 5a). The lengths were measured

between the intersections of the tangential rises, starting from the minimum, and the tangents, running to the surface of the specimen (Fig. 5b). Using the diameter, it was possible to quantify the different damages caused by the applied impact loads. As the results were reproducible, this sole criterion is seen as sufficient for the purpose of this investigation.

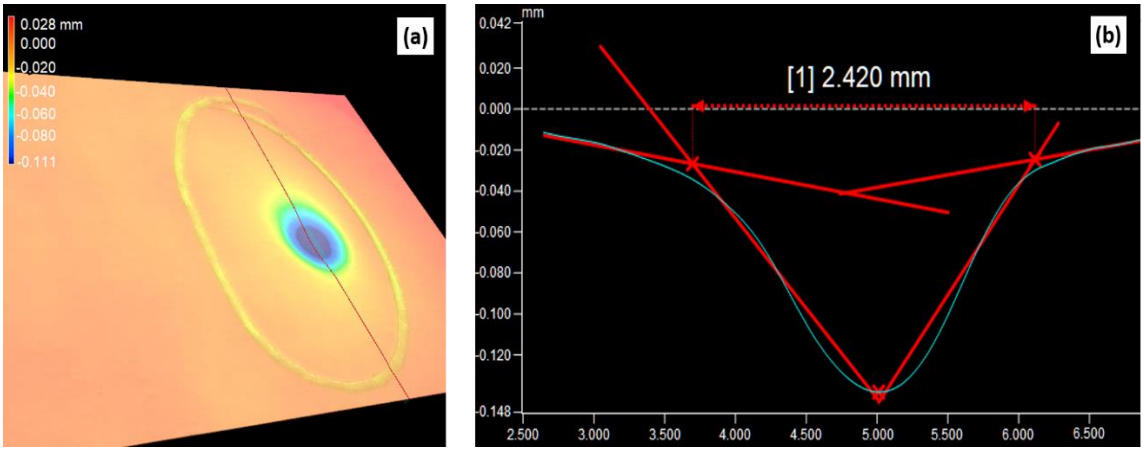

Fig. 5. Topographic scan of specimen's imprint (a); virtual cross-section through the imprint (b)

The resulting damage on the specimens was analyzed qualitatively and quantitatively by the help of statistical tests. The Shapiro-Wilks-Test was implemented to investigate the data's normal distribution. Hereinafter, a Mann-Whitney U-Test (Cohen 2013) was calculated to determine whether there were differences in the mean imprint diameter between Material A - 330 and Material B - 350 at pressure levels of 0.1, 0.15, and 0.2 MPa.

The data collection, management, and visualization as well as statistical computations were performed using the following software-tools: Microsoft Excel (Microsoft Corporation, Version 2208, Redmond, WA, USA), Wolfram Mathematica (Wolfram Research, Version 11.1.1., Champaign, IL, USA), RStudio-Cloud (RStudio, Version 2022 online, Boston, Ma, USA), and JASP (Version 0.16.3, Amsterdam, Netherlands).

RESULTS AND DISCUSSION

Damage Phenomena

The measurements showed that the increase in the velocities and the kinetic energy of the impactor resulted in different damage phenomena. The qualitative assessment of the damage phenomena was performed by digital analysis of the ruptured areas of the specimens. A categorical classification of the incurred damage phenomena of the investigated cardboard materials is presented in Fig. 6, where the height profiles of the damage phenomena are shown. The blue color on the top side of the specimen signalizes high deformation in the depth, while the red color indicates the reference surface. In contrast, the red and blue color on the bottom side signify deformation in the height and the reference surface, respectively.

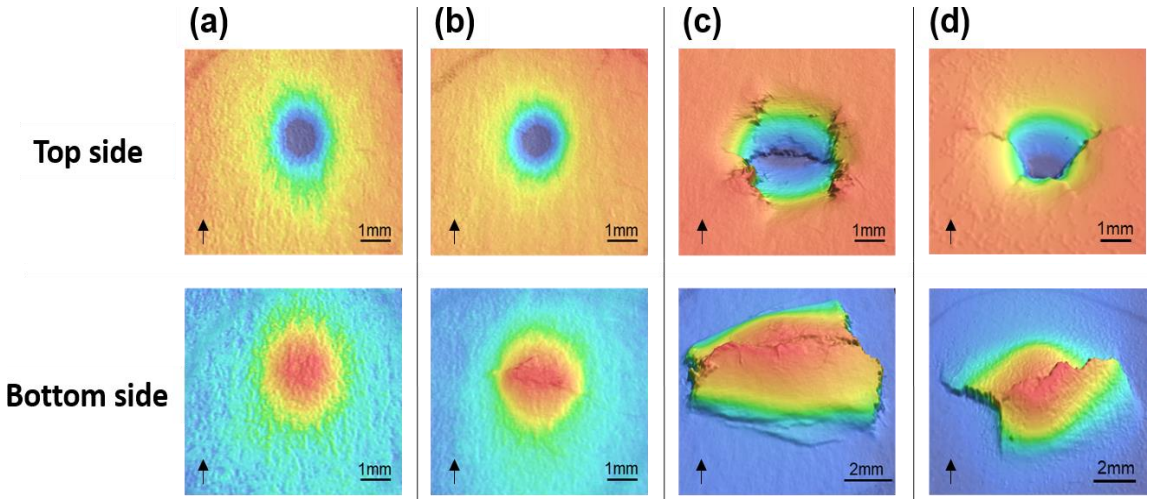

Fig. 6. Different damage phenomena: Imprint (a), Crack (b), and Breakthrough (c) of Material B - 350 as well as Breakthrough of Material A - 330 (d) caused by variously dynamic loads taken by a 3D-macroscope

The following three different damage phenomena were identified: *Imprint (I)* implies that a plastic deformation is detectable on the material surface. However, no layer is completely ruptured (Fig. 6a). *Cracking (C)* signifies that one layer on the surface of the material is damaged through high bending forces (Fig. 6b). *Breakthrough (B)* means that all layers of the specimen are damaged (Fig. 6c and Fig. 6d).

The qualitative comparison of the occurring damages after the impact showed a similar behavior between Material A - 330 and Material B - 350. It was recognizable that the first crack occurred on the bottom of the material due to high bending forces, which might be associated with attenuated hydrogen bonds that led to a rupture of the fiber structure of the layer. These phenomena were detectable on the bottom sulphate pulp layer of Material B - 350 and the light coating layer of Material A - 330. In the stage of breakthrough, it was noticeable that the crack on the bottom side was always perpendicular to the fiber direction of the specimen. This appeared independent of the investigated material.

However, another distinct breakthrough behavior was also observed. While Material B - 350 tended to tear completely without deformation on the top side (Fig. 6Fig.c), Material A - 330 was characterized by deformation (Fig. 6d). This pattern could have resulted from different layer composition of the materials. In addition, it was found that the perpendicular cracks to the fiber direction differed in the crack length, which could possibly be explained by the anisotropy or varying strength of the fiber structure.

Table 2 summarizes the percentage shares of damage phenomena that occurred for Material A - 330 and Material B - 350. The values were calculated based on the number of impacts and the observed damage pattern on the specimens at respective pressure settings.

A change in the distribution of the damage phenomenology with different pressure settings was recognizable. As expected, a continuing increase in the pressure resulted in an increase in breakthroughs and a decrease in cracks and imprints for both materials.

Table 2. Damage Phenomena at Respective Pressure Settings

	Material A - 330							
Pressure (MPa)	0.05	0.08	0.09	0.10	0.11	0.12	0.15	0.20
Number of Impacts	20	19	20	18	20	20	18	20
Velocity *u* (m/s)	18.77	24.59	26.25	27.25	29.28	30.56	33.09	38.24
I - Imprint (%)*	100	42	35	39	15	5	0	0
C - Crack (%)*	0	32	45	33	40	15	6	0
B - Breakthrough (%)*	0	26	20	28	45	80	94	100
	Material B - 350							
Pressure (MPa)	0.10	0.13	0.14	0.15	0.16	0.20	0.30	
Number of Impacts	19	17	18	18	16	17	16	
Velocity *u* (m/s)	27.25	31.55	32.86	33.44	35.33	38.14	44.53	
I - Imprint (%)*	100	53	22	45	6	0	0	
C - Crack (%)*	0	12	28	22	0	0	0	
B - Breakthrough (%)*	0	35	50	23	94	100	100	
* Percentage of damage phenomena								

Resulting Mean Imprint Diameter

Figure 7 shows the development of the mean imprint diameter and its scatter over the impactor's kinetic energy of Material A - 330 in which the typical damage stages are highlighted. The formation of a transition area reveals that at least two different damage phenomena occurred. The standard deviation at pressure settings of 0.12 MPa and 0.15 MPa was at a high level before the transition to the breakthrough stage.

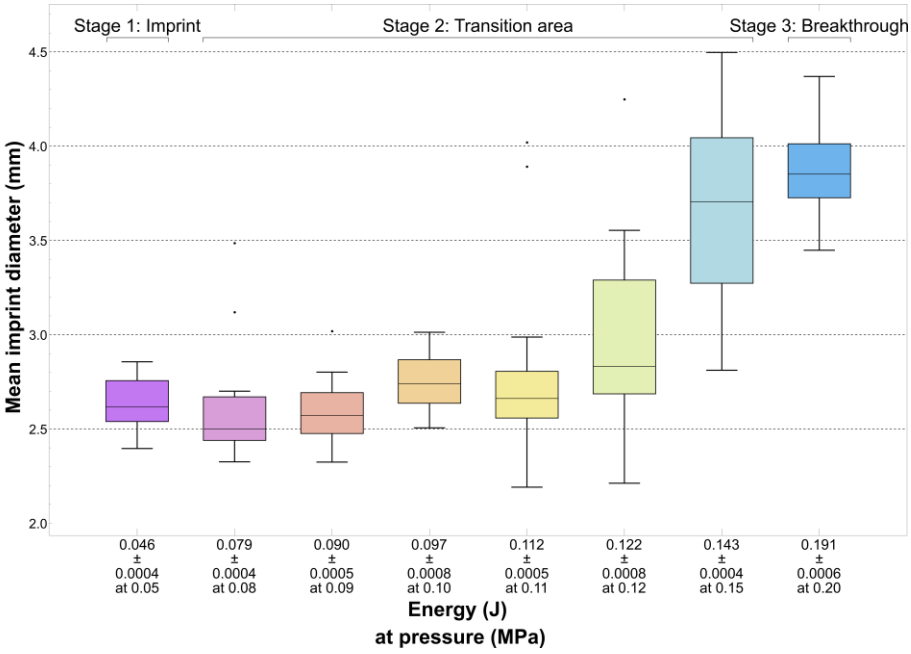

Fig. 7. Typical damage stages – Imprint (I), Transition area (I, C, B), Breakthrough (B) - of Material A - 330 at respective pressure settings

Figure 8 shows the development of the mean imprint diameter and its scatter over the impactor's kinetic energy of Material B - 350. The typical damage stages are implemented as well. Similarly, the standard deviation at the pressure setting of 0.16 MPa was at a high level before the onset of the breakthrough stage.

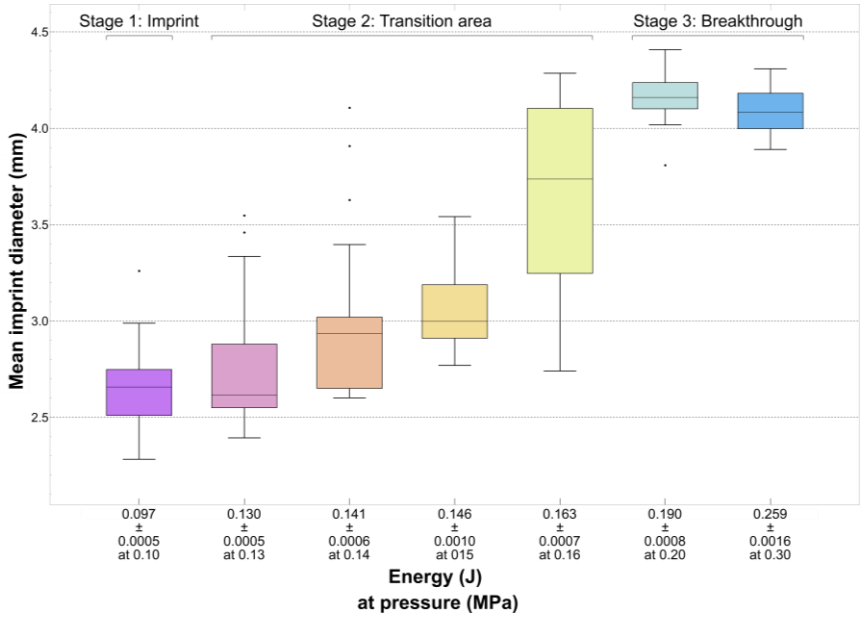

Fig. 8. Typical damage stages – Imprint (I), Transition area (I, C, B), Breakthrough (B) - of Material B - 350 at respective pressure settings

Comparing Mean Imprint Diameter

The resulted imprint diameters ($\boldsymbol{D_{imp}}$) corresponding to the pressure settings (see Figs 7 and 8) are ideally reproduced by a nonlinear asymmetric sigmoidal function, as defined by Eq. 2,

$$D_{\text{imp}} = f(E) = d + \frac{a-d}{\left(1+\left(\frac{E}{c}\right)^{b}\right)^{m}} \quad (2)$$

where *a*, *b*, *c*, *d*, and *m* are free parameters. These parameters were determined by means of a least squares approach. The material specific parameters for Material A - 330 and Material B - 350 are presented in Table 3.

Table 3. Material Specific Parameters and Sigmoidal Function

Parameter	Material A - 330	Material B - 350
a	2.64	2.68
b	11.32	14.12
c	0.27	0.27
d	3.88	4.13
m	1719.78	1712.61
$\boldsymbol{D_{\text{imp}}}$	$3.88 + \frac{2.64-3.88}{\left(1+\left(\frac{E}{0.27}\right)^{11.32}\right)^{1719.78}}$	$4.13 + \frac{2.68-4.13}{\left(1+\left(\frac{E}{0.27}\right)^{14.12}\right)^{1712.61}}$

Figure 9 shows the function graphs for both Material A - 330 and Material B - 350. The obtained quantitative results of the impact tests indicate that the relationship between the mean imprint diameter and the applied kinetic energy functions was similar for both types of material. A change in the increase of the curve correlated with a change in the typical damage stage.

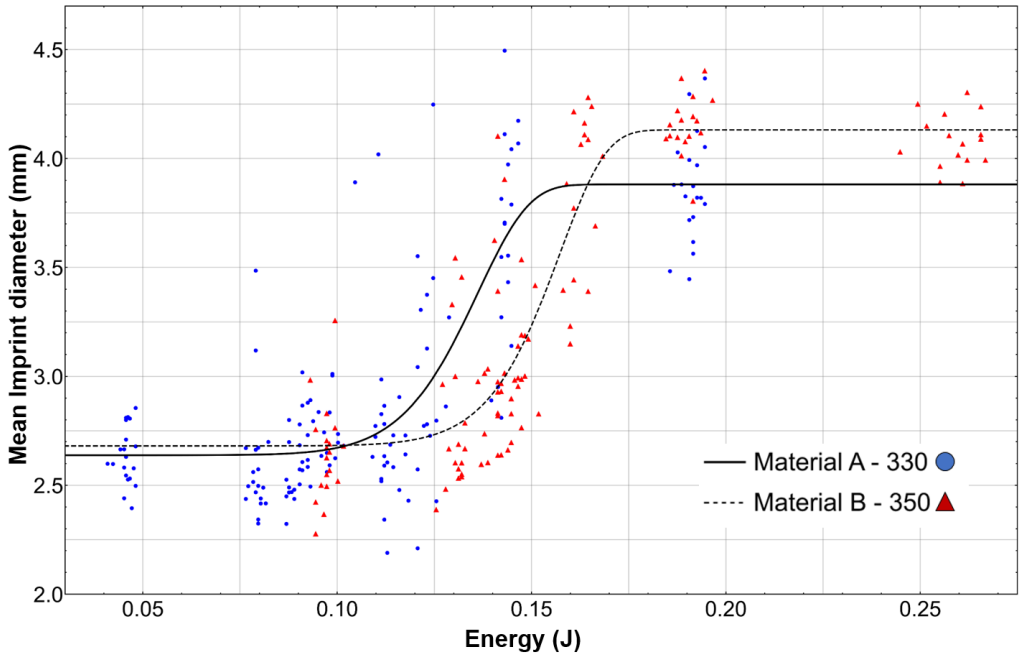

Fig. 9. Comparison of the approximated sigmoidal functions for Material A - 330 and Material B **-** 350

Before running an independent samples t-test, the Shapiro-Wilks-Test was performed. As a result, the distribution of the imprint diameter for Material A - 330 and Material B - 350 deviated from normality at all pressure levels. Thus, a Mann-Whitney U-Test was calculated to investigate the differences in the mean imprint diameter of Material A - 330 and Material B - 350 (Cohen 2013).

At a pressure of 0.1 MPa (equivalent to 0.097 J), the differences of the mean imprint diameter of Material A - 330 (M = 2.75; SD = 0.15) and Material B - 350 (M = 2.65; SD = 0.22) were marginally significant (U = 235.00; $p < .10$). At a pressure of 0.15 MPa (equivalent to 0.142 J), the mean imprint diameter of Material A - 330 (M = 3.64; SD = 0.48) was higher than the mean diameter of Material B - 350 (M = 3.04; SD = 0.21). The difference was significant as well (U = 272.00; $p < .001$), and there was a strong positive effect (Cohen's d = 0.68). There was a statistically significant difference in mean imprint diameter between Material A - 330 (M = 3.87; SD = 0.24) and Material B - 350 (M = 4.16; SD = 0.14) at a pressure of 0.2 MPa (U = 50.00; $p < .001$). Further, there was a strong negative effect (d = -0.71). This implies that the mean imprint diameter of Material B - 350 tends to be larger than the imprint diameter of Material A - 330 at a pressure level of 0.2 MPa (equal to 0.19 J). Comparing pressure level 0.15 MPa and 0.2 MPa, contradictory effects were statistically observed in the behavior of the mean imprint diameter of Material A - 330 and Material B - 350. This pattern could also be confirmed by the approximated sigmoidal functions (see Fig. 9). This result can be explained by the different layer composition of Material A - 330 and Material B - 350.

Three different stages of damage could be identified that are characteristic to all test specimens. The transition area extended over a similarly large energy range for Material A - 330 and Material B - 350. However, different kinetic energies could be recognized, which caused various damage phenomena on the specimens. Further, a lower

kinetic energy between imprint and transition stages was observed in Material A - 330 compared to Material B - 350. This was also the case during the change from the transition stage to the breakthrough stage (see Fig. 9). The cardboard with the structure and composition of Material B - 350 seems to be more resistant to bending forces. Thus, Material B - 350 showed higher impact load resistance.

Material A - 330 and Material B - 350 have a different structure. However, the total thickness as well as the grammage of the layers was higher in Material B - 350 than in Material A - 330. This also resulted in the different impact resistances. It can be assumed that it also increases with an increase in basis weight, which Bivainis and Jankauskas (2015) also described. They investigated the impact load behavior of corrugated board using puncture tests. Although the cardboard and corrugated board had different material compositions, a similar relationship pattern could be observed. However, this correlation can only be confirmed in the present investigation as a tendency, because different materials of different grammage were measured.

In some cases, there was a discrepancy between the determined imprint diameters on the specimens at identical kinetic energy impact load. Such mismatch between the diameters could result from the tightly elastic properties and anisotropy in the materials, which demonstrates different behavior under impact loads. The anisotropy is due to the manufacturing process of the board. The fibers are all oriented in the same way in the material. If the material gets damaged, the anisotropy can cause the material to behave differently in different directions when it breaks.

Limitations and Future Implications

In this investigation, a current and permanent state of damage patterns after impact were obtained. Therefore, interpretations about damage progressions cannot be made. However, the results help to understand the behavior of different cardboard materials under impact loads. This knowledge is particularly important for designing and for developing further packaging material with suitable layer composites and layer thickness. Material manufacturers and producers need to pay attention to the requirements of the material, thus, enhancing the properties of these composites to better resist external influences during transport. Based on the discussed safety aspects of the experimental setup it would be possible to safely use the proposed test rig and demonstrated evaluations approach in addition to a conventional cardboard manufacturing process.

Regarding the various and sometimes unpredictable behavior patterns of composite material under impact loads, further experimental research should focus on the occurrence probabilities of certain types of damage. In particular, different cardboard materials should be compared in terms of imprints, cracks, and breakthroughs under various, experimentally controlled circumstances (air humidity, temperature, *etc.*).

To keep the future experimental effort low and to enable a numerical analysis of different cardboard materials under impact loads, it is also recommended to set up a simulation model. Therefore, the current experimental data on the impact behavior can be used to understand the governing impact phenomena and to verify dynamic finite element analyses (FEA) of cardboard materials. However, for this purpose, further experimental tests, such as tensile tests at the high strain rates (Ebert *et al.* 2011) and multistep stress-relaxation tests, are required to complete classification according to Haupt (1993) and the description of the material behavior.

CONCLUSIONS

1. Three different damage phenomena of cardboard materials under impact load have been identified: imprint, cracking, and breakthrough. These damage phenomena were similar in Material A - 330 and Material B - 350.
2. Differences in the damage pattern were detected in the breakthrough area. While Material B - 350 cracked, Material A - 330 experienced additional deformation in the form of local curvatures around the point of impact.
3. The necessary kinetic impact energies to cause structural damage were determined for both materials. Depending on the structure of the material, the required impact load was different for the tested materials.
4. A characteristic nonlinear asymmetric sigmoidal function of the mean imprint diameter behavior with increasing kinetic energies was observed.
5. The obtained results show that the impact load resistance of Material B - 350 was better than Material A - 330. It can be assumed that the impact load resistance increases with increasing grammage. However, this would have to be investigated further.

ACKNOWLEDGMENTS

The authors are grateful for the support of the Open Access Publication Funds of the HTWK Leipzig.

REFERENCES CITED

Baumann, G. (2016). *Logistische Prozesse: Berufe der Lagerlogistik*, Bildungsverlag EINS, Troisdorf, Germany.

Bivainis, V., and Jankauskas, V. (2015). "Impact of corrugated paperboard structure on puncture resistance," *Materials Science* 21(1), 37-61. DOI: 10.5755/j01.ms.21.1.5713

Coffin, D. W., Gustafsson, P.-J., Hägglund, R., Kulachenko, A., Mäkelä, P., Nygards, M., Östlund, S., Uesaka, T., Niskanen, K., Berglund, L., and Carlsson, L. A. (2011). *Mechanics of Paper Products*, DE GRUYTER, Berlin, Boston. DOI: 10.1515/9783110254631

Cohen, J. (2013). *Statistical Power Analysis for the Behavioral Sciences*, Routledge, New York, United States of America.

Corner, E., and Paine, F. A. (2002). *Market Motivators: The Special Worlds of Packaging and Marketing*, CIM, Cookham, England.

DIN EN ISO 534 (2012). "Paper and board - Determination of thickness, density and specific volume," Deutsches Institut für Normung [German Institute for Standardisation], Berlin, Germany.

Ebert, C., Hufenbach, W., Langkamp, A., and Gude, M. (2011). "Modelling of strain rate dependent deformation behaviour of polypropylene," *Polymer Testing* 30(2), 183-187. DOI: 10.1016/j.polymertesting.2010.11.011

Garbowski, T., Gajewski, T., and Grabski, J. (2020). "Estimation of the compressive strength of corrugated cardboard boxes with various openings," *Energies* 14(1), 155. DOI: 10.3390/en14010155

Garbowski, T., Gajewski, T., and Knitter-Piątkowska, A. (2022). "Influence of analog and digital crease lines on mechanical parameters of corrugated board and packaging," *Sensors* 22(13), article 4800. DOI: 10.3390/s22134800

Garbowski, T., Maier, G., and Novati, G. (2012). "On calibration of orthotropic elastic-plastic constitutive models for paper foils by biaxial tests and inverse analyses," *Structural and Multidisciplinary Optimization* 46(1), 111–128. DOI: 10.1007/s00158-011-0747-3

Griffin, R. C., Sacharow, S., and Brody, A. L. (1985). "Materials and package testing," in: *Principles of Package Development*, Springer Netherlands, Dordrecht, 130-167. DOI: 10.1007/978-94-011-7382-7_5

Haupt, P. (1993). "On the mathematical modelling of material behavior in continuum mechanics," *Acta Mechanica* 100(3–4), 129–154. DOI: 10.1007/BF01174786

Herzau, E., Kaßmann, M., and Volkmann, F. (2010). *Verpackungsprüfung*, Beuth Praxis, Beuth, Berlin Wien Zürich.

ISO 187 (2022). "Paper, board and pulps – Standard atmosphere for conditioning and testing and procedure for monitoring the atmosphere and conditioning of samples," International Organization for Standardization, Geneve, Switzerland.

Kaeppeler, U., Schneller, K., Wallburg, F., Engisch, L., and Schönfelder, S. (2022). "Analysis of the compression behavior of different cardboard materials during embossing," *Open Conference Proceedings* 2, 129-135. DOI: 10.52825/ocp.v2i.132

Käppeler, U., Berlich, A., and Engisch, L. (2019). *Charakterisierung Physikalisch, Chemischer Veränderungen im Karton im Ultraschallunterstützten Prägeprozess*, Master's Thesis, University of Applied Sciences, Leipzig, Germany.

Käppeler, U., Hünniger, J., Hofmann, A., Hamblyn, S., Berlich, A., and Engisch, L. (2020). "Chemical and morphological changes in fibre structure due to material heating during ultrasonic-assisted embossing of cardboard," *BioResources* 16(1), 546-557. DOI: 10.15376/biores.16.1.546-557

Luong, V., Bonnin, A.-S., Abbès, F., Nolot, J.-B., Erre, D., and Abbès, B. (2021). "Finite element and experimental investigation on the effect of repetitive shock in corrugated cardboard packaging," *Journal of Applied and Computational Mechanics* 7(2). DOI: 10.22055/jacm.2020.35968.2771

Luong, V. D., Abbès, F., Abbès, B., Duong, P. T. M., Nolot, J.-B., Erre, D., and Guo, Y.-Q. (2018). "Finite element simulation of the strength of corrugated board boxes under impact dynamics," in: *Proceedings of the International Conference on Advances in Computational Mechanics 2017*, Lecture Notes in Mechanical Engineering, H. Nguyen-Xuan, P. Phung-Van, and T. Rabczuk (eds.), Springer Singapore, Singapore, 369-380. DOI: 10.1007/978-981-10-7149-2_25

Mrówczyński, D., Garbowski, T., and Knitter-Piątkowska, A. (2021). "Estimation of the compressive strength of corrugated board boxes with shifted creases on the flaps," *Materials*, 14(18), 5181. DOI: 10.3390/ma14185181

Pålsson, H. (2018). *Packaging Logistics: Understanding and Managing the Economic and Environmental Impacts of Packaging in Supply Chains*, New York, NY : Kogan Page, London, England.

Ran, J., and Liu, C. (2019). "Modeling of the stiffness of corrugated cardboard considering material non-linear effect," *Journal of Physics: Conference Series*, 1187(3), article 032069. DOI: 10.1088/1742-6596/1187/3/032069

Singh, P., Wani, A. A., and Langowski, H.-C. (eds.). (2017). *Food Packaging Materials: Testing & Quality Assurance*, CRC Press, Boca Raton, United States of America.

Statista. (2022). "Produktionsmenge ausgewählter Papier- und Pappewaren in Deutschland bis 2020," *Statista*, (https://de-statista-com.ezproxy.htwk-leipzig.de/statistik/daten/studie/240921/umfrage/produktionsmenge-ausgewaehlter-papier-und-pappewaren/), Accessed 21 Jan 2023.

Weber, P., Wolf, J., Stephan, B., and Hauptmann, M. (2022). "Experimental investigation towards the transport-optimized design of peelable polymer tray packaging," *Packaging Technology and Science*, pts. 2649. DOI: 10.1002/pts.2649

Article submitted: December 10, 2022; Peer review completed: January 7, 2023; Revised version received and accepted: January 22, 2023; Published: January 24, 2023.
DOI: 10.15376/biores.18.1.1933-1947
ERRATUM: April 26, 2023; Columns in Table 3 were re-labeled for accuracy. This change does not alter any results or conclusions.